



Effective xylan integration for remodeling biochar uniformity and porosity to enhance chemical elimination and CO₂ adsorption

Yongtai Wang^{a,b,1}, Huiyi Zhang^{a,b,1}, Yunong Li^{a,b}, Hua Yu^b, Dan Sun^b, Yujing Yang^b, Ran Zhang^a, Li Yu^c, Fei Ma^c, Muhammad Nauman Aftab^d, Liangcai Peng^{a,b}, Yanting Wang^{a,b,*}

^a College of Plant Science & Technology, Huazhong Agricultural University, Wuhan 430070, China

^b Key Laboratory of Fermentation Engineering (Ministry of Education), Hubei Key Laboratory of Industrial Microbiology, School of Life & Health Sciences, Hubei University of Technology, Wuhan 430068, China

^c Oil Crops Research Institute of the Chinese Academy of Agricultural Sciences, Wuhan 430062, China

^d Institute of Industrial Biotechnology, Govt. College University, Lahore 54000, Pakistan

ARTICLE INFO

Keywords:

Plant evolution
Diverse lignocelluloses
Xylan interlink
Chemical adsorption
Carbon neutralization

ABSTRACT

Although plant evolution has offered diverse biomass resources, the production of high-quality biochar from desirable lignocelluloses remains unexplored. In this study, distinct lignocellulose substrates derived from eight representative plant species were employed to prepare biochar samples under three different temperature treatments. Correlation analysis showed that only hemicellulose was a consistently positive factor of lignocellulose substrates to account for the dye-adsorption capacities of diverse biochar samples. Furthermore, we integrated *exo*-xylan, a major hemicellulose in higher plants, into lignin-disassociated lignocelluloses to produce the desirable biochar with a uniform and symmetrical structure, resulting in a 5.2-fold increase in surface area (51 to 317 m²/g) and a 5.0-fold increase in total pore volume (0.02 to 0.11 cm³/g micropore, 0.02 to 0.12 cm³/g mesopore). This consequently improved the adsorption capacities of the remodeled biochar, with an increase of 26 % for dual-industry dyes, 90 % for 1579 organic compounds, and 14 % for CO₂. Based on the fluorescence observation of xylan-cellulose co-localization and physical-chemical characterization of the remodeled biochar, a novel hypothetical model was proposed to explain how xylan plays an integral role in desired biochar production, providing insights into effective lignocellulose reconstruction and efficient thermochemical catalysis as an integrative strategy to maximize biochar adsorption capacity.

1. Introduction

Through photosynthesis, plants capture atmospheric carbon to produce carbohydrates including starch-rich foods and lignocellulose-based biomass resources [1]. Although plant cell walls represent the most convertible biomass resource for renewable biofuels and valuable bio-products, plants have evolved diverse cell walls that enable them to adapt to various aqueous and terrestrial environments [2]. However, the complex structures and multiple biological functions of plant cell walls account for lignocellulose recalcitrance to the enzymatic hydrolysis and chemical catalysis of biomass [3]. Hence, lignocellulose recalcitrance not only increases the cost of biomass processing but also releases secondary waste into the environment [4].

Plant cell walls are primarily composed of cellulose, hemicellulose, and lignin, with small amounts of pectic polysaccharides and wall proteins [5]. In general, plant cell wall composition and features dynamically diverge from lower to higher plants, enabling sustained plant growth and development under various ecological conditions and geographic locations [6]. As the chief hemicellulose in higher plants, xylan positively affects enzymatic saccharification of biomass by reducing cellulose crystallinity in bioenergy crops [7]. Since the amorphous/non-crystalline chains of cellulose microfibrils have recently been identified as breakpoints for initiating and completing lignocellulose enzymatic hydrolysis and chemical conversion, it is assumed that xylan may be involved in interactions with amorphous cellulose chains to preserve cellulose nanofibril assembly in plant cell

* Corresponding author at: Key Laboratory of Fermentation Engineering (Ministry of Education), Hubei Key Laboratory of Industrial Microbiology, School of Life & Health Sciences, Hubei University of Technology, Wuhan 430068, China.

E-mail address: wyt@mail.hzau.edu.cn (Y. Wang).

¹ Equal contribution

<https://doi.org/10.1016/j.ijbiomac.2024.138865>

Received 5 June 2024; Received in revised form 25 November 2024; Accepted 15 December 2024

Available online 16 December 2024

0141-8130/© 2024 Published by Elsevier B.V.

walls [8,9]. Although xylan plays a positive role in the biochemical conversion of lignocellulose substrates into biofuels, little is known about the function of hemicellulose in thermochemical conversion for highly valuable bioproduction.

Lignocellulose-derived biochar has emerged as a green strategy for multiple applications in agriculture, industry, and the environment [10,11]. In particular, biochar is increasingly being utilized to remove toxic chemicals from factory sites and for CO₂ adsorption to reduce the net carbon release into the environment [12]. Over the past few years, attempts have been made to produce high-performance biochar by improving the thermochemical catalysis of lignocellulose substrates [13]. The physicochemical properties of biochar include surface area, pore size distribution, functional groups, and cation exchange capacity [14]. Although diverse lignocellulose substrates have been used to produce biochar, the mechanism by which lignocellulose composition and features determine biochar properties and quality under various thermochemical conversion conditions remains unknown [15].

Physical and chemical pretreatments have been widely performed to reduce lignocellulose recalcitrance and enhance sequential biomass enzymatic saccharification [16,17]. However, they release toxic biochemicals that inhibit microbial fermentation during the final biofuel production [18]. Therefore, biochar is considered an effective biosorbent for eliminating toxic chemicals. In this study, we collected distinct lignocellulose substrates from eight plant species that represented the evolution from lower to higher plants (Fig. S1). To avoid any external chemical activation impact on lignocellulose carbonization, this study focused on producing biochar samples by simply performing thermal treatments with those eight lignocellulose substrates under three temperatures (400, 600, and 800 °C), and then detected biochar adsorptive capacities with industry dyes. Based on the correlation analysis, we identified hemicellulose as a consistently positive factor accounting for biochar adsorption capacity compared to other wall polymers of lignocellulose substrates. Furthermore, by employing exogenous xylan in an *in vitro* model of plant cell walls for biochar production, we demonstrated that hemicellulose dynamically improved biochar porosity to extensively increase biochar adsorption of either industrial dyes, phenolic compounds, and diverse organic chemicals from biomass pretreatments or environmental CO₂. Finally, we proposed a mechanistic model that links all the major findings of this study to interpret the major role of xylan in biochar production with a relatively high adsorption capacity.

2. Material and methods

2.1. Collection of biomass samples

Chlorella powder was purchased from Shengqing Biotechnology Co., Ltd. (Xi'an, China), and the stem tissues of moss (*Hypnum plumaeforme*) and fern (*Adiantum capillus-veneris*) were obtained from Shangcheng County, Xinyang, China. Straws and stem tissues were collected from corn (Z31) [1], wheat (ZM9023) [16], poplar (*Populus nigra*) [19] and rice cultivar (NPB) and its mutant (*Osf16*) [20] grown in the experimental fields of Huazhong Agricultural University, Wuhan, China. Stem tissues of eucalyptus (*Eucalyptus 3229*) [19] were collected from Guangdong Eucalyptus Germplasm Field, Zhanjiang, China. All mature tissues were dried at 55 °C, ground through a 40-mesh screen, and stored in a dry container until in use.

2.2. Wall polymers extraction and determination

Plant cell wall fractionation was performed as described previously [21]. An ultraviolet-visible (UV-VIS) spectrometer (V-1100D; Shanghai MAPADA Instruments Co.) was used for hexose, pentose, and uronic acid assays, as previously described [22]. The total lignin content was determined using a two-step acid hydrolysis method according to the Laboratory Analytical Procedure of the National Renewable Energy

Laboratory [23].

2.3. Monosaccharides and cellulose feature assays

The monosaccharides of the wall polysaccharides were determined using gas chromatography–mass spectrometry (GC–MS) (Shimadzu GCMS-QP2010 Plus) with *myo-inositol* as the internal standard [24]. The cellulose crystalline index (CrI) was determined using the X-ray diffraction method [25]. The degree of polymerization (DP) of cellulose was measured using viscometry [26].

2.4. Molecular weight assay of xylan samples

The molecular weights of various xylan fractions were measured using size-exclusion chromatography with multi-angle laser-light scattering and refractive index detection (SEC-MALLS-RI) as previously described [27].

2.5. Immunolocalisation of xylan and cellulose

Co-immunolocalization of xylan and cellulose was performed as previously described [28] with minor modifications. Approximately 10 mg of the biomass sample was incubated with a diluted antibody solution (LM11 against xylan, Leeds University), a secondary antibody (anti-rat IgG, Invitrogen) linked to fluorescein isothiocyanate (FITC), and S4B (Sigma-Aldrich, Missouri, USA) [29]. Fluorescence was observed using a microscope with epifluorescence irradiation and differential interference contrast (DIC) optics (NE910; Yong Xin Optics Co., Ltd., Zhejiang, China). Images were captured using a Hamamatsu ORCA285 camera and Improvision Velocity software. Fluorescence intensities were calculated using ImageJ software (National Institutes of Health, Maryland, USA).

2.6. Biochar preparation

Approximately 2 g of the biomass sample was placed in a tube furnace (OTF-1200×) that had been heated to a certain temperature, as described previously [30] with minor modifications. The biomass carbonization was processed under N₂ at a rate of 5 °C min⁻¹ and heated to 400, 600, or 800 °C for 2 h, and then cooled down to 300 °C at a rate of 10 °C min⁻¹. After cooling to room temperature, the carbon residues were collected, washed with 1 M HCl aqueous solution for 6 h, and then washed with double-distilled water until at neutral pH value.

2.7. Preparation of xylan-modified biomass samples for biochar production

The crude cell walls of the rice straw were termed as *Rice-Raw*, and extracted as described: (1) The *Rice-Raw* was suspended in 4 M KOH (containing 1.0 mg mL⁻¹ sodium borohydride) for 1 h at 25 °C, and the residues were obtained by centrifugation at 3000 xg for 5 min, and washed with 75 % ethanol until pH 7 as the rice xylan-removed residue sample (termed as deXylan for its biochar). (2) In a parallel experiment, the total solution (supernatant and residue) after 4 M KOH extraction of rice straw was directly added with anhydrous ethanol (3:1, v/v), vortexed for 10 min, and incubated at 4 °C for 72 h. After the supernatant was removed, the remaining residue was washed with 75 % ethanol until the pH reached 7 to obtain a rice xylan-recovery residue sample (termed de-xylan-recovery). (3) The rice xylan-recovery residues were respectively added with commercial *exo*-xylan (Macklin Biochemical Co., Ltd., Shanghai, China) at four proportions (1:1, 3:1, 5:1, and 7:1; w/w), vortexed for 10 min and incubated at 4 °C for 72 h. After the supernatants were removed, the remaining residues were washed with 75 % ethanol to pH 7 as an *exo*-xylan-supplemented xylan-recovery residue sample (termed de-Xylan-recovery@Xylan). All xylan-modified biomass samples were applied to produce biochar using the 600 °C treatment as

described above.

2.8. Analysis of biochar adsorption with dyes and phenols

Methylene blue (MB) and Reactive Blue 19 (RB19) were prepared by adding $C_{16}H_{18}ClN_3S$ and $C_{22}H_{16}N_2Na_2O_{11}S_3$, respectively, into ultra-pure water at room temperature (25 ± 2 °C). After mixing 20 mL of the dye and 20 mg of biochar, batch adsorption experiments were performed for 12 h under 150 rpm shaking. After stirring, the samples were filtered through a 0.45 μ m membrane filter, and the concentration of the residual dye in the filtrate was determined using a UV–VIS spectrometer (V–1100D, Shanghai MAPADA Instruments Co.) at $\lambda_{max} = 668$ nm and 595 nm as described [31,32]. The equilibrium adsorption capacity (q_e , mg g⁻¹) was determined using eq. (1):

$$q_e = \frac{(C_0 - C_e)V}{W} \quad (1)$$

where C_0 and C_e were the initial and equilibrium solution concentrations of the dyes (mg L⁻¹), respectively; V (L) was the volume of the solution; and W (g) was the weight of the biochar used. Approximately 20 mL phenol (1 g L⁻¹) solution was incubated with 20 mg biochar for 12 h under 150 rpm shaking as performed with dyes above and measured at $\lambda_{max} = 270$ nm [33].

The adsorption kinetics were fitted using pseudo-first- and pseudo-second-order kinetics. The Langmuir and Freundlich models were fitted to the adsorption equilibrium data [34].

2.9. Total organic carbon (TOC) adsorption analysis

Another adsorption experiment was performed with biochemicals released from alkali and acid (NaOH, H₂SO₄) pretreatments with rice (NPB) straw. The chemical pretreatments with rice straw were conducted as previously described [35]. For NaOH pretreatment, the straw powder was supplemented with 6 mL 1 % NaOH (w/v). For H₂SO₄ pretreatment, the powder was added with 6 mL 1 % H₂SO₄ (v/v) and heated at 121 °C for 20 min in an autoclave. The samples were then shaken at 150 r/min for 2 h at 50 °C, and centrifuged at 3000 xg for 5 min. About 20 mL supernatants of the pretreatments were added with 20 mg of biochar samples, and batch adsorption experiments were performed for 12 h under 150 rpm shaking. After stirring, the samples were filtered through a 0.45 μ m membrane filter. Residual total organic carbon (TOC) concentration in the filtrate was determined using a TOC analyzer (Multi N/C 3100, Analytik Jena, Germany), and the equilibrium adsorption capacity (q_e , mg g⁻¹) was determined using eq. (1). Organic compounds in the pretreatment supernatants were detected using an ultra-high-performance liquid chromatography coupled with quadrupole/electrostatic field orbitrap high-resolution mass spectrometry (UPLC-Orbitrap-MS) system (UPLC/Vanquish, MS/HFX) and a Q-Exactive HFX Hybrid Quadrupole Orbitrap mass spectrometer equipped with a heated electrospray ionization (ESI) source (Thermo Scientific), as previously described [36].

2.10. CO₂ capture analysis

The CO₂ capture capacity was measured using an Autosorb IQ MP (Quantachrome Instruments, USA) at 0 °C and 25 °C, respectively, and the CO₂ adsorption isotherm curve was acquired by testing at two temperatures and a pressure range of 0–1 bar. The capacity of the sample was calculated according to the adsorption isotherm as previously described [37].

2.11. Characterization of biomass and biochar samples

The biomass and biochar samples were characterised using the volumetric method (ASAP 2460, Micromeritics, USA), scanning electron

Table 1

Cell wall composition (% dry matter) of eight plant species.

Sample	Hemicellulose	Cellulose	Lignin	Pectin
Chlorella	5.40 ± 0.28	2.59 ± 0.09	ND	0.66 ± 0.02
Moss	10.83 ± 0.54	14.53 ± 0.51	ND	1.11 ± 0.09
Fern	11.15 ± 0.30	26.35 ± 0.70	40.97 ± 2.87	1.23 ± 0.05
Corn	15.93 ± 0.81	22.34 ± 1.01	16.34 ± 0.91	0.88 ± 0.14
Wheat	20.83 ± 0.99	30.79 ± 1.45	22.73 ± 1.02	1.35 ± 0.10
Rice	17.89 ± 0.65	20.04 ± 1.05	14.72 ± 0.37	0.76 ± 0.04
Eucalyptus	13.59 ± 0.17	30.74 ± 0.60	25.54 ± 0.66	1.13 ± 0.09
Poplar	13.58 ± 0.47	32.28 ± 0.79	28.73 ± 1.86	1.81 ± 0.04
Median	13.59	24.35	24.14	1.12
CV (%)	32.72	41.57	37.19	32.46

Data as mean ± SD ($n = 3$), ND as non-detectable; CV as coefficient of variation.

microscopy (GeminiSEM 300, ZEISS, Germany), X-ray photoelectron spectroscopy (K-Alpha, Thermo Scientific, USA), diffraction of X-rays (SmartLab SE, Rigaku, Japan), Raman spectra (Alpha300R, WITec, Germany), and Fourier transform infrared (FTIR, Nicolet iS 10, Thermo Scientific, USA) attenuated total reflection (ATR) spectroscopy.

2.12. Statistical analysis

Student's *t*-test and analysis of variance (ANOVA) were performed using the SPSS 23 software (IBM, USA). The line graph, histogram, and regression analysis for the best-fit curve were plotted using the Origin software (OriginLab, USA).

3. Results and discussion

3.1. Diverse lignocellulose resources for biochar production

We collected eight lignocellulose substrates from three representative lower plants and five higher plants, because plant evolution drives diverse plant cell walls that enable adaptation to various environmental conditions. Higher plants represent major global crops (corn, wheat, and rice) and forestry trees (eucalyptus and poplar), whereas the three lower plants cover both aquatic and terrestrial plants. Using the well-established method, we determined the cell wall composition of mature stem tissues from eight plant species (Table 1). Plants exhibited large variations in the levels of the four wall polymers, with coefficient variations (CVs) ranging from 32 % to 42 %. Cellulose levels varied from 3 % to 32 % (% dry matter), whereas non-cellulosic polysaccharide (hemicellulose or pectin) levels showed relatively less variation. Furthermore, we examined many more variations in the monosaccharide proportions of non-cellulosic polysaccharides in the eight plant species, with CVs ranging from 64 % to 154 % (Table S1), suggesting that hemicellulose variation is a major cause of plant cell wall evolution [38]. The five higher plants had much higher proportions of xylose and arabinose, confirming that xylan is the predominant hemicellulose in higher plants [39,40]. Additionally, we detected two key features of cellulose (CrI and DP). With CVs of 32 % and 36 % (Table S2), the eight plants showed relatively fewer variations in CrI and DP values, respectively, compared to that of the monosaccharide proportions of the non-cellulosic polysaccharides. Hence, these eight plant species represented diverse lignocellulose substrates and provided prominent biomass resources for bioenergy crops for biochar production.

3.2. Adsorptive performances of biochar produced from lignocellulose resources

Using eight plant species of diverse lignocellulose composition, this study performed thermal treatments with those biomass substrates to produce biochar under three temperatures (400 °C, 600 °C and 800 °C) without any extra chemical activation, then detected biochar adsorption capacity with methylene blue (MB), a typically cationic dye designed to

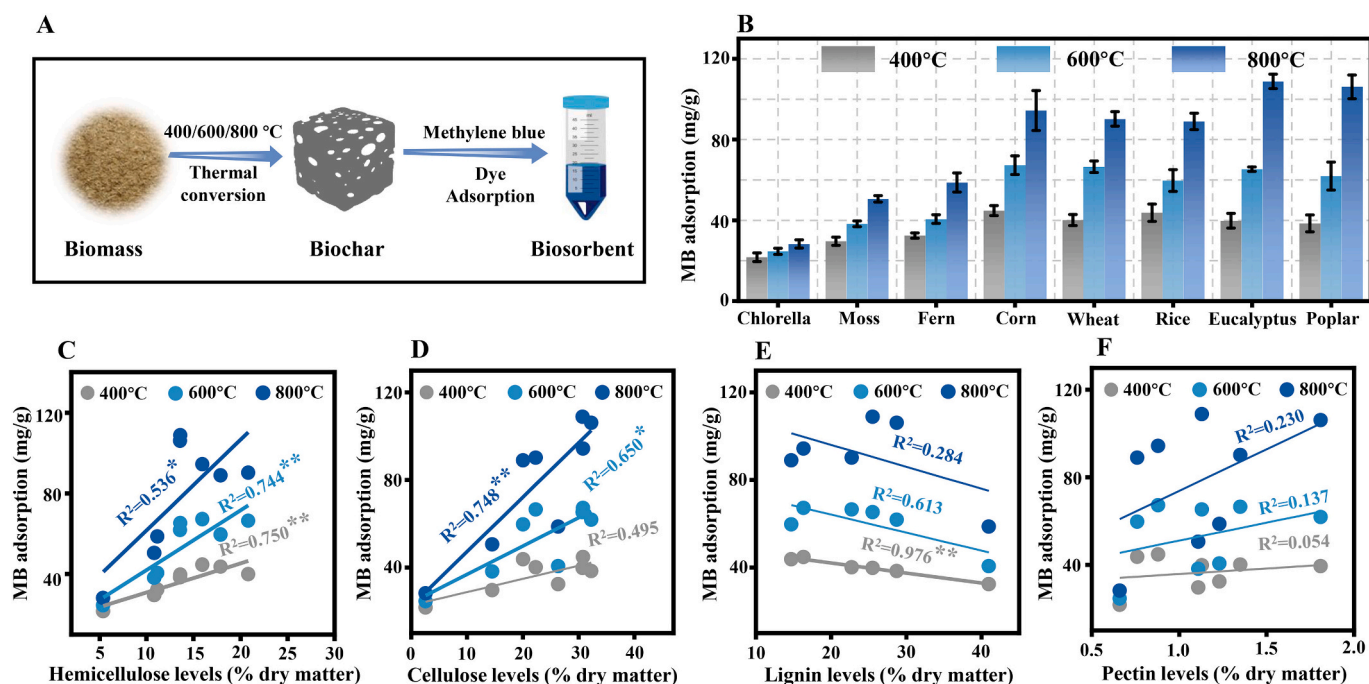


Fig. 1. Distinct biochar production from eight diverse lignocellulose substrates for MB dye adsorption. (A) Experimental procedure; (B) MB adsorption with the biochar obtained from eight plant lignocelluloses, bar as mean \pm SD ($n = 3$); (C, D, E & F) Correlation analysis between wall polymer levels and MB adsorption capacity. * and ** as significant correlations at $p < 0.05$ and 0.01 ($n = 8$, except for lignin $n = 6$), respectively.

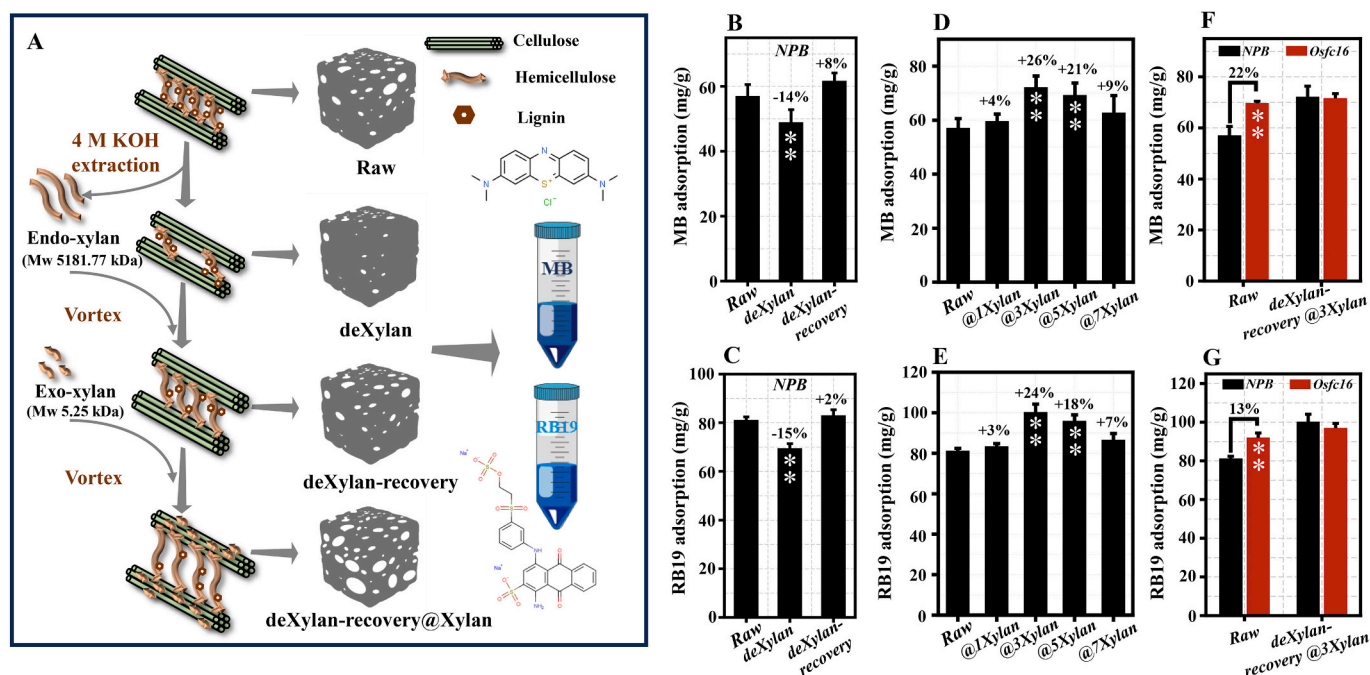


Fig. 2. Xylan-modified lignocellulose substrates for distinct remodeled-biochar production with high dye-adsorption. (A) The schematic diagram for major experiments conducted; (B-G) Biochar adsorption capacities with two industry dyes (MB, RB19); Data as mean \pm SD ($n = 3$); ** As a significant difference between remodeled-biochar and control biochar (Raw) by t -test at $p < 0.01$ ($n = 3$) and % calculated by subtraction between remodeled-biochar and control one (Raw) divided by Raw; NPB as rice cultivar (wild type/WT) and *Osf16* as *OsCESA9* site-mutant.

indicate the typical wall polymer role in biochar adsorption (Fig. 1A). As the thermal-treatment temperatures were increased from 400 °C to 800 °C, all biochar samples showed a consistently higher MB adsorption capacity. However, that of the five higher plants remained much higher than that of lower plants, particularly for the two woody plants at 800 °C (Fig. 1B), suggesting a distinctive biochar production from diverse

lignocellulose substrates of the eight plant species. Furthermore, we conducted a correlation analysis between biochar dye adsorption capacity and lignocellulose composition in the eight plant species examined (Fig. 1C-F). As a comparison, hemicellulose levels exhibited a consistently positive correlation with biochar samples produced under three temperatures at $p < 0.05$ or 0.01 ($n = 8$) (Fig. 1C), whereas the

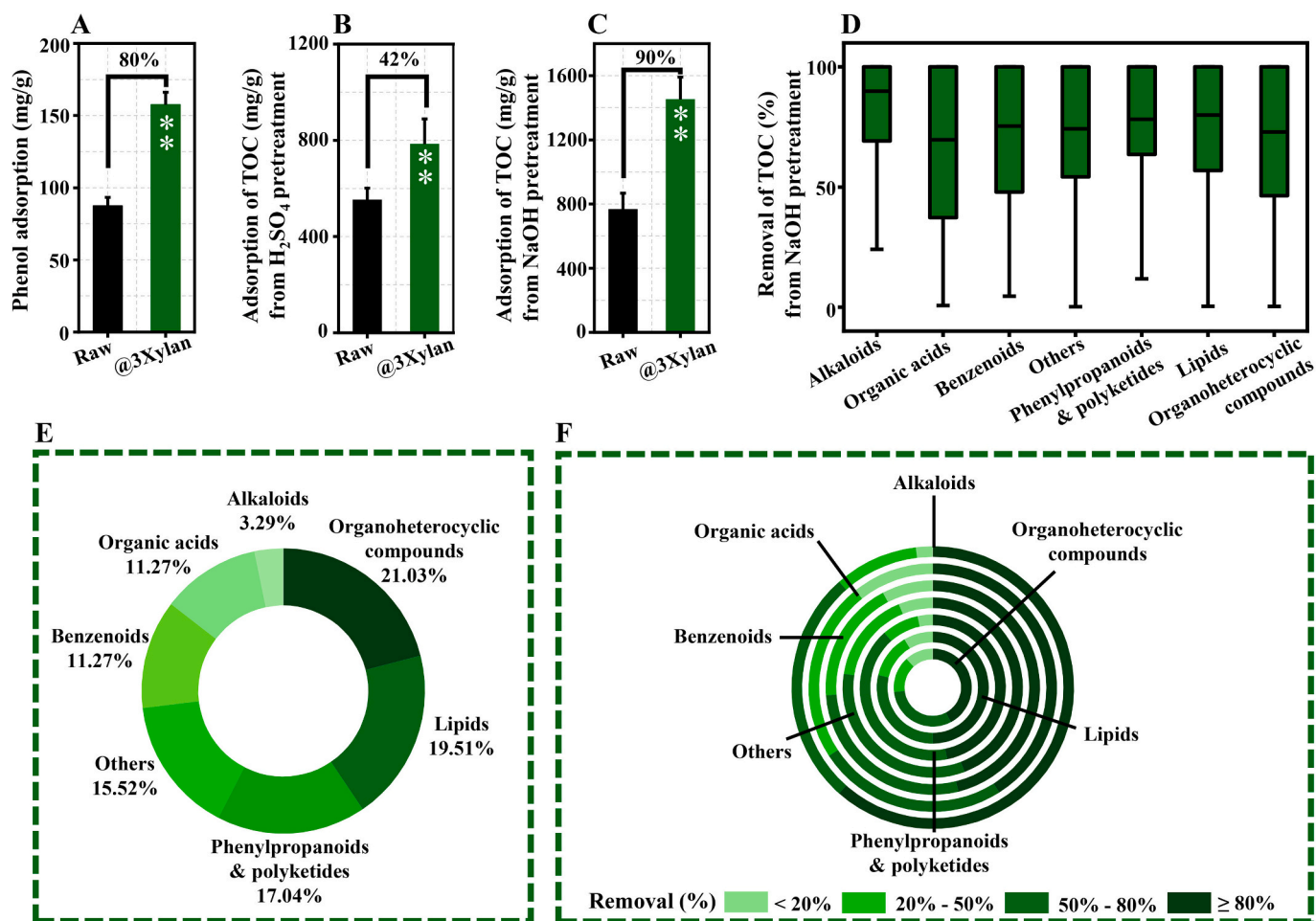


Fig. 3. Xylan-remodeled biochar adsorption with organic chemicals. Adsorption capacities with commercial phenol (A) and total organic carbon (TOC) released from rice (NPB) biomass pretreatments with acid (B) and alkali (C); TOC from chemical pretreatment supernatant; (D) Removal rate of seven types of organic compounds (released from alkali pretreatment) after remodeled-biochar adsorption; (E) The proportion of seven organic compounds of the total; (F) Removal proportions (%) of seven organic compounds; Bar as mean \pm SD ($n = 3$); ** As significant difference between the two samples by t -test at $p < 0.01$ ($n = 3$) and % calculated by subtraction between remodeled-biochar and control one (Raw) divided by Raw; @3Xylan as 3-fold *exo*-xylan remodeled-biochar and Raw as control biochar as termed in Fig. 2.

cellulose or lignin levels only had a significantly positive or negative correlation with the biochar samples produced under two temperatures (600 °C and 800 °C) (Fig. 1D) or one temperature (400 °C) (Fig. 1E), suggesting that the hemicellulose played a consistently positive role in biochar production for high dye adsorption. In contrast, the correlation analyses also indicated that cellulose at a low temperature (400 °C) and lignin at high temperatures (600 °C and 800 °C) play minor roles in high biochar adsorption with MB dye. In addition, pectin levels did not show any significant correlation (Fig. 1F), mainly because of their low levels in all eight plant species examined. Hence, as the biochar samples were produced without any additional chemical activation, the results demonstrated the consistently positive role of hemicellulose in enhancing biochar adsorption capacity [14,41,42].

3.3. Dynamic enhancement of dye adsorption by xylan-modified biochar

To test the positive role of hemicellulose in biochar production for high dye adsorption, we initially performed 4 M KOH extraction to remove 67 % xylan from rice cultivar (NPB) straw and measured the molecular weight of the extracted *endo*-xylan (Mw 5181.77 kDa, Mn 485.32 kDa, and Mw/Mn 10.68). After xylan removal, the remaining residue was used to produce biochar at 600 °C (deXylan sample) and biochar adsorption capacity with MB and reactive blue-19 (RB19), another anionic dye, was examined (Fig. 2A). In comparison, the

deXylan biochar showed significantly lower adsorption capacities with MB and RB19 than the control biochar (Rice-Raw) at $p < 0.01$ level ($n = 3$) (Fig. 2B & C), which was consistent with correlation result about the hemicellulose level as a positive factor for biochar adsorptive capacity (Fig. 1C). Although 4 M KOH extraction partially removed xylan and small lignin from lignocellulose [43], the remaining lignin levels in the KOH-extracted residues did not show any significant correlation with dye adsorption capacities of the biochar samples produced from these lignocellulose residues under 600 °C treatment (Fig. 1E). This suggests that the reduced dye adsorption capacities in the deXylan biochar, compared with raw biochar, should be primarily due to xylan removal rather than the lignin coextraction. To test this finding, we used xylan-recovered lignocellulose substrate to produce a biochar sample (termed as deXylan-recovery), and then detected slightly increased adsorption capacities for MB and RB19 dyes compared to that of the raw biochar, providing dual evidence of the positive role of hemicellulose deposition in biochar production for high dye adsorption capacity.

To confirm the role of hemicellulose in biochar production, we further obtained other four biochar samples (deXylan-recovery@1,3,5,7Xylan) by supplying exogenous xylan (Mw 5.25 kDa, Mn 3.67 kDa, and Mw/Mn 1.43) into the xylan-recovered lignocellulose substrates at different proportions (1-, 3-, 5- and 7 fold; w/w). Compared with the raw biochar (control sample), the four deXylan-recovery@Xylan biochar samples all showed much higher adsorption

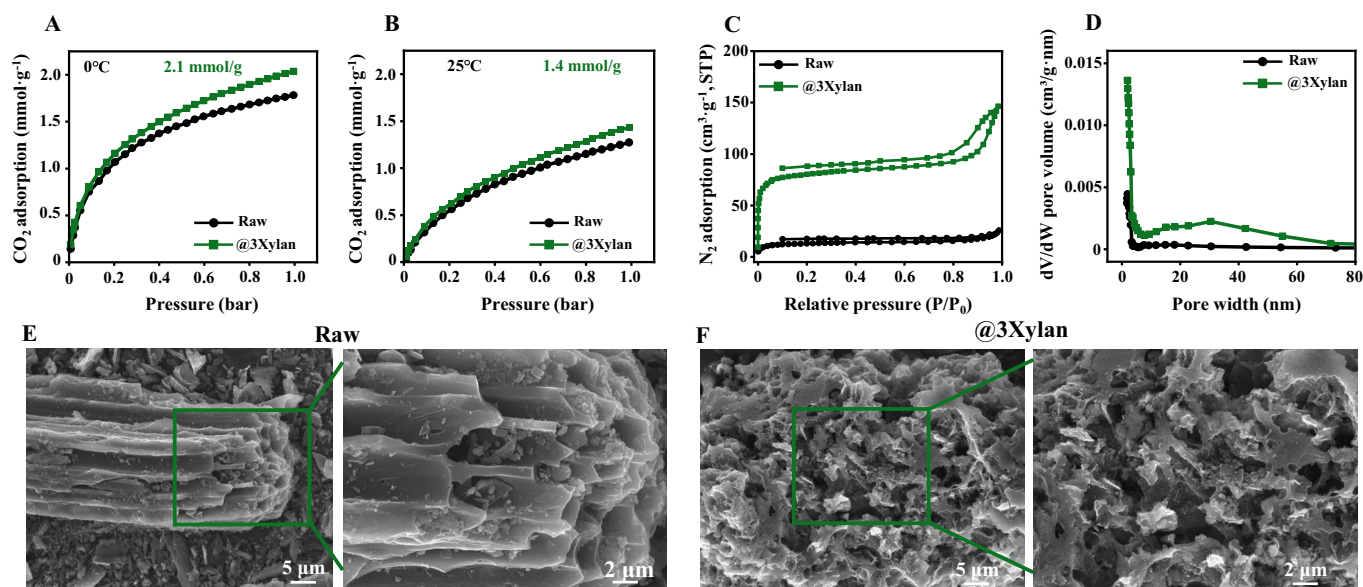


Fig. 4. Characterization of biochars for porosity. (A, B) CO₂ capture with biochars under 0 °C and 25 °C, respectively; (C) N₂ adsorption-desorption isotherm; (D) BJH adsorption micropore distribution; (E, F) SEM images. @3Xylan as 3-fold exo-xylan remodeled-biochar and Raw as control biochar as termed in Fig. 2.

capacities for MB and RB19 dyes (Fig. 2D & E), which confirmed that the hemicellulose supplement could consistently improve their biochar production for dye adsorption. Given the 3-fold exo-xylan supplementation resulted in the biochar with the highest dye adsorption capacity, this study found that 5- and 7-fold exo-xylan supplementations did not further improve biochar production, along with slightly reduced adsorption capacities relative to the 3-fold sample, indicating a dynamic impact of exo-xylan deposition on biochar production. This also suggests that excessive xylan deposition may significantly alter lignocellulose homogeneity and integrity, leading to an adverse impact on biochar production [44].

Concerning the dynamic impacts of exo-xylan supplements on biochar production, we also obtained the biochar sample at 600 °C by employing our previously identified rice mutant (*Osf16*), which had much increased hemicellulose proportion in lignocellulose substrate of mature straw (Fig. S2) [20]. Importantly, the mutant biochar sample exhibited 22 % and 13 % higher adsorption capacities for MB and RB19 dyes, respectively, compared with the wild-type (NPB) sample ($p < 0.01$, $n = 3$) (Fig. 2F & G). This is likely due to the higher proportion of hemicellulose in mutant lignocellulose applied for biochar production. This finding confirmed the positive role of hemicellulose deposition in biochar production for high dye adsorption. However, by supplying 3-fold exo-xylan to the mutant lignocellulose substrate, we determined a similar adsorption capacity between the mutant and NPB samples, providing further evidence that excessive xylan deposition did not significantly affect the biochar adsorption capacity.

Furthermore, the isothermal adsorption curves and fitting parameters of the two dyes were obtained using the control (raw) and modified biochar (@3Xylan) samples (Fig. S3A & B; Table S3). In comparison, the Langmuir model showed much higher R^2 values (> 0.99), whereas the Freundlich model maintained R^2 values from 0.93 to 0.99. Based on the adsorption kinetic curves and fitting parameters (Fig. S3C & D; Table S4), the two biochar samples rapidly adsorbed most dyes within 60 min and then entered a slow adsorption stage until equilibrium. Compared with the pseudo-first-order model, the adsorption was better fitted by the pseudo-second-order model, suggesting a multifaceted adsorption mechanism consisting of both monolayer and multilayer adsorption processes driven by chemical interactions and the incorporation of physical adsorption. This observation implies that both the specific surface area and abundance of surface functional groups of biochar materials are major factors accounting for dye adsorption

capacity, which further clarifies how the modified biochar was of enhanced dye adsorption capacity [45]. Therefore, it is assumed that hemicellulose deposition plays a central role in biochar production for highly adsorptive performance.

3.4. Enhanced organic chemical adsorption with biochar

Because the biochar sample obtained from the 3-fold exo-xylan supplement (@3Xylan) had the highest adsorption capacity for two industrial dyes relative to the control (Raw) sample as described above, we also examined its adsorption capacities for organic chemicals (Fig. 3). In general, the modified biochar (@3Xylan) sample showed significantly higher adsorption capacities for phenol and two sources of total organic carbon (TOC) released from acidic (H₂SO₄) and alkaline (NaOH) pretreatments with mature rice straw by 42 %–90 %, compared to the control (raw) biochar sample (Fig. 3A–C). As the TOC composition released from alkali pretreatment was identified using LC-MS, 1579 compounds could be adsorbed by the modified biochar, and those compounds were classified into seven types of chemicals including alkaloids (52, 3.29 %), organic acids (178, 11.27 %), benzenoids (195, 15.52 %), phenylpropanoids and polyketides (269, 17.04 %), lipids (308, 19.51 %), organoheterocyclic compounds (332, 21.03 %), and others (245, 15.52 %) (Fig. 3D–F). Among the 1579 adsorptive compounds, approximately 77 % compounds had adsorption capacities over 50 %, but the adsorption capacities of 46 % of the compounds reached 80 %, revealing that the xylan-modified biochar had excellent adsorption capacities for a wide range of organic compounds from biomass processing. Given that biochar has a high adsorption capacity for organics [46], this study also examined efficient adsorption with pretreatment compounds, probably resulting from the generation of more active groups during the alkali pretreatment performed.

3.5. Uniform structure of modified biochar for higher porosity

As carbon materials are increasingly considered promising adsorbents for CO₂ capture, this study also tested modified biochar adsorption with CO₂ at two representative temperatures (0 °C and 25 °C) under atmospheric pressure (1 bar) (Fig. 4A & B). In comparison, the modified biochar showed a consistently higher CO₂ adsorption capacity than the control biochar sample, suggesting that the modified biochar had a relatively higher porosity, as described previously [47]. This study thus

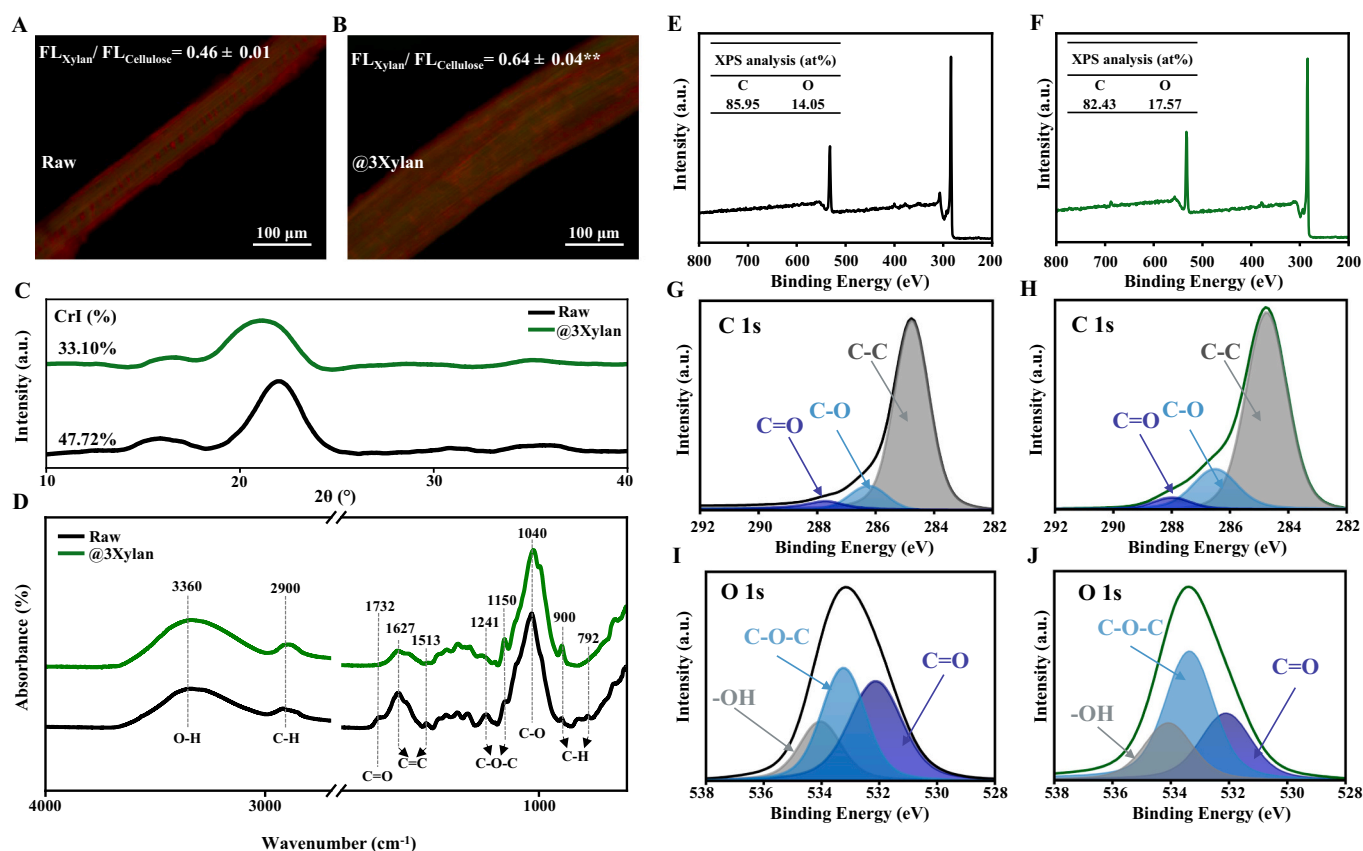


Fig. 5. Characterization of biomass and biochars of xylan-modified and control (Raw) samples. (A, B) Observation *in situ* of xylan and cellulose immunolocalization in lignocellulose substrates, the data of fluorescence intensities measured as mean \pm SD ($n = 3$), ** As significant difference between the two samples by *t*-test at $p < 0.01$ ($n = 3$); (C) XRD patterns with CrI values of lignocellulose samples; (D) FTIR profiling as annotated in Table S5 of lignocellulose samples; (E, F) XPS scan spectra profiling of biochar samples; (G–J) XPS of C 1s & O 1s spectra.

measured the porosity and observed the morphology of the two biochar materials to understand the modified biochar with high capacities for diverse chemical removal and CO₂ capture (Fig. 4C–F). Based on BET analysis, the modified biochar showed consistently higher N₂ adsorption and pore volume than the control biochar (Fig. 4C & D), which is in agreement with the CO₂ adsorption capacity examined above. At low relative pressures (below 0.02), the N₂ adsorption capacity of modified-biochar (@3Xylan) was up to 6-fold higher than that of control biochar (Raw), implying that the modified biochar was rich in micropores. The modified biochar had a typical hysteresis loop, which may result from narrow cylindrical pores, whereas the control biochar (Raw) had slit-shaped pores [48]. The data suggest that xylan deposition not only increases the pore size of biochar but may also reshape its pore structure, thereby leading to an integrative enhancement of adsorption capacity. The control biochar (Raw) sample exhibited an uneven distribution with a partially plant-vascular-tissue-like structure. In contrast, the modified biochar (@3Xylan) sample was uniformly and symmetrically constructed with a sponge-like structure (Fig. 4E & F). Notably, the specific surface area of the modified biochar reached 317 m²/g, which was significantly higher than that of the control biochar by 5.2-fold (Fig. S4A). Similarly, the

volumes of three types of pores consistently increased by 4.5–5.0-fold in the modified biochar relative to the control sample (Fig. S4B–D), confirming that the increased pore volumes were responsible for the enlarged specific surface area of the modified biochar sample. However, to maximize biochar porosity by exploring the optimal *exo*-xylan supplementation and biochar production conditions should be investigated in future studies.

3.6. Characterization of xylan-modified lignocellulose substrate for high-performance biochar production

To understand how xylan-modified lignocellulose is favored for high-performance biochar construction, we observed xylan and cellulose distribution *in situ* in the lignocellulose substrate supplemented with 3-fold *exo*-xylan based on fluorescence localization using a specific antibody (LM11/green) against xylan or S4B dye (red) staining with cellulose microfibrils (Fig. 5A, B & Fig. S5). In general, both raw lignocellulose and xylan-supplemented samples exhibited a fully fluorescent distribution of xylan and cellulose in all tissues examined. However, compared to the raw lignocellulose, the xylan-modified lignocellulose showed significantly increased fluorescence intensities for either xylan and cellulose deposition or the xylan/cellulose ratio at $p < 0.01$, providing evidence of the extensive *exo*-xylan distribution and interaction with cellulose microfibrils. To confirm this finding, we determined a significantly reduced cellulose CrI value of 44 % in the xylan-modified lignocellulose compared with that in raw lignocellulose (Fig. 5C), which should be partially accounting for the *exo*-xylan interaction with cellulose microfibrils *via* hydrogen bonds [7,24]. Under Fourier transforms infrared (FT-IR) spectroscopy, we further observed relatively reduced intensities of chemical bonds in the modified lignocellulose such as peaks at 782 cm⁻¹ (C–H vibration of the aromatic ring), 1241 cm⁻¹ (C–O–C stretching of aryl-alkyl ether), 1513/1627 cm⁻¹ (C=C stretching of the aromatic ring), and 1732 cm⁻¹ (C=O stretching of acetyl or carboxylic acid), whereas the intensities were increased about the hemicellulose and cellulose at 900 cm⁻¹ (C–H vibration), 1040 cm⁻¹ (C–O stretching), 1150 cm⁻¹ (C–O–C asymmetric stretching), 2900 cm⁻¹ (C–H stretching), and 3360 cm⁻¹ (O–H

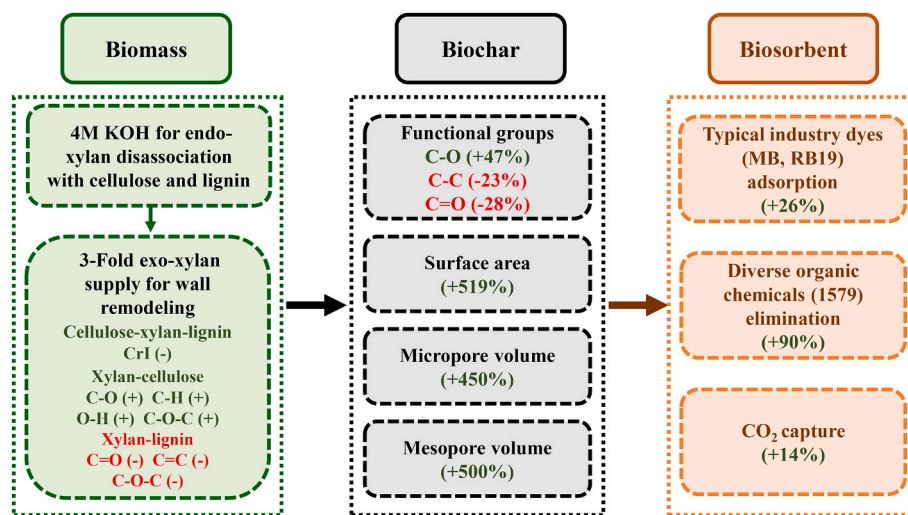


Fig. 6. A mechanism model to elucidate how xylan acts as a central link for lignocellulose modification enabled the remodeling of biochar with raised porosity accountable for extensively enhanced adsorption capacities with two industry dyes, diverse organic compounds, and CO₂. (+) and (–) as increased and decreased parameter/rates; Green and Red were highlighted as positive and negative factors.

stretching) (Fig. 5D; Table S5). Although the increase in chemical groups suggests a possible interaction between exo-xylan and native cellulose microfibrils in the xylan-modified lignocellulose substrate, further investigation is required to confirm this.

Furthermore, we determined the elemental composition and chemical characteristics of the biochar samples by X-ray photoelectron spectroscopy (XPS) (Fig. 5E–J). Compared with the control (Raw), the xylan-modified biochar sample contained less carbon at 82.43 %, with a relatively higher proportion of oxygen at 17.57 %, indicating that more oxygen-containing functional groups were present in the modified biochar. By estimating three peaks in C 1 s (C–C/284.8 eV, C–O/286.4 eV, C=O/287.9 eV) and three peaks for O 1 s (C=O/531.7 eV, C–O–C/533.0 eV, –OH/534.0 eV) [49,50], the xylan-modified biochar showed a much-raised proportion of the C–O group and relatively reduced C–C and C=O groups, compared to the control biochar (Table S6). Using X-ray diffraction (XRD) and Raman spectroscopy, we found that both the control and xylan-modified biochar samples had similar graphite and crystalline properties (Fig. S6), suggesting that exo-xylan supplementation may mainly improve the biochar structure and porosity rather than its graphitizing properties.

Based on the major findings of this study, we proposed a hypothetical model to interpret how exo-xylan supplementation enhanced the xylan-cellulose interaction in the modified lignocellulose substrate, thereby improving the biochar structure and porosity to account for the high adsorption capacity for diverse organic chemicals and CO₂ (Fig. 6). The initial 4 M KOH extraction and recovery should mainly disassociate the endo-xylan from cellulose and lignin, enabling 67 % of the exo-xylan to interact with native cellulose microfibrils for wall-network remodel. This explains why the xylan-modified lignocellulose had a reduced CrI value because of the increased xylan-cellulose association via hydrogen bonds and other possible interlinks, as well as the reduced xylan-lignin association [51]. Because xylan plays a central role in uniform and symmetrical carbon construction, it would be interesting to explore specific xylan involvement in lignocellulose carbonization. Given that this study was originally designed to focus on xylan's specific role in biochar production, chemical coactivation could be explored in the future to further improve the biochar structure for maximizing its adsorption capacity.

4. Conclusion

We performed a simple thermal conversion to produce distinct

biochar samples by using diverse lignocelluloses from plant evolution, and identified hemicellulose as a consistently positive factor for biochar production. We achieved a sponge-like biochar with a uniform and symmetrical structure for upgraded porosity accountable for raised 5.2-fold surface area and 4.5–5.0 folds micropore/mesopore volumes by supplying low-molecular-weight exo-xylan to reconstruct lignocellulose substrates. The modified biochar was further detected with significantly enhanced adsorption capacities for diverse chemical elimination or CO₂ capture. We thus propose a novel model for xylan as a central interlink of lignocellulose substrate for desired biochar production, revealing a powerful strategy for high-performance biochar construction by integrating xylan-modified lignocellulose with an effective thermochemical process.

CRediT authorship contribution statement

Yongtai Wang: Writing – original draft, Methodology, Investigation, Formal analysis. **Huiyi Zhang:** Writing – review & editing, Methodology, Investigation, Formal analysis. **Yunong Li:** Validation, Methodology, Formal analysis. **Hua Yu:** Writing – review & editing, Methodology. **Dan Sun:** Methodology, Formal analysis. **Yujing Yang:** Methodology, Formal analysis. **Ran Zhang:** Validation, Methodology, Investigation. **Li Yu:** Supervision, Methodology. **Fei Ma:** Methodology, Formal analysis. **Muhammad Nauman Aftab:** Methodology, Formal analysis. **Liangcai Peng:** Writing – review & editing, Supervision, Funding acquisition, Conceptualization. **Yanting Wang:** Writing – review & editing, Supervision.

Declaration of competing interest

The authors declare that they have no known competing financial interests or personal relationships that could have appeared to influence the work reported in this paper.

Acknowledgments

This work was in part supported by the Hubei Provincial Natural Science Foundation of China for Excellent Young Scientists (2024AFA100); National Natural Science Foundation of China (32470273, 32170268, 32101701), the National 111 Project of the Ministry of Education of China (BP0820035), and the Initiative Grant of Hubei University of Technology for High-level Talents (GCC20230001).

Appendix A. Supplementary data

Supplementary data to this article can be found online at <https://doi.org/10.1016/j.ijbiomac.2024.138865>.

Data availability

Data will be made available on request.

References

- L. Wu, S. Feng, J. Deng, B. Yu, Y. Wang, B. He, H. Peng, Q. Li, R. Hu, L. Peng, Altered carbon assimilation and cellulose accessibility to maximize bioethanol yield under low-cost biomass processing in corn brittle stalk, *Green Chem.* 21 (16) (2019) 4388–4399, <https://doi.org/10.1039/C9GC01237K>.
- Z.A. Popper, Evolution and diversity of green plant cell walls, *Curr. Opin. Plant Biol.* 11 (3) (2008) 286–292, <https://doi.org/10.1016/j.pbi.2008.02.012>.
- Y. Wang, P. Liu, G. Zhang, Q. Yang, J. Lu, T. Xia, L. Peng, Y. Wang, Cascading of engineered bioenergy plants and fungi sustainable for low-cost bioethanol and high-value biomaterials under green-like biomass processing, *Renew. Sust. Energ. Rev.* 137 (2021) 110586, <https://doi.org/10.1016/j.rser.2020.110586>.
- C. Gong, L. Cao, D. Fang, J. Zhang, M. Kumar Awasthi, D. Xue, Genetic manipulation strategies for ethanol production from bioconversion of lignocellulose waste, *Bioresour. Technol.* 352 (2022) 127105, <https://doi.org/10.1016/j.biortech.2022.127105>.
- Y. Li, P. Liu, J. Huang, R. Zhang, Z. Hu, S. Feng, Y. Wang, L. Wang, T. Xia, L. Peng, Mild chemical pretreatments are sufficient for bioethanol production in transgenic rice straws overproducing glucosidase, *Green Chem.* 20 (9) (2018) 2047–2056, <https://doi.org/10.1039/C8GC00694F>.
- L. Wu, M. Li, J. Huang, H. Zhang, W. Zou, S. Hu, Y. Li, C. Fan, R. Zhang, H. Jing, L. Peng, S. Feng, A near infrared spectroscopic assay for stalk soluble sugars, bagasse enzymatic saccharification and wall polymers in sweet sorghum, *Bioresour. Technol.* 177 (2015) 118–124, <https://doi.org/10.1016/j.biortech.2014.11.073>.
- F. Li, M. Zhang, K. Guo, Z. Hu, R. Zhang, Y. Feng, X. Yi, W. Zou, L. Wang, C. Wu, J. Tian, T. Lu, G. Xie, L. Peng, High-level hemicellulosic arabinose predominantly affects lignocellulose crystallinity for genetically enhancing both plant lodging resistance and biomass enzymatic digestibility in rice mutants, *Plant Biotechnol. J.* 13 (4) (2015) 514–525, <https://doi.org/10.1111/pbi.12276>.
- R. Zhang, Z. Hu, H. Peng, P. Liu, Y. Wang, J. Li, J. Lu, Y. Wang, T. Xia, L. Peng, High density cellulose nanofibril assembly leads to upgraded enzymatic and chemical catalysis of fermentable sugars, cellulose nanocrystals and cellulase production by precisely engineering cellulose synthase complexes, *Green Chem.* 25 (3) (2023) 1096–1106, <https://doi.org/10.1039/D2GC03744K>.
- R. Zhang, Z. Hu, Y. Wang, H. Hu, F. Li, M. Li, A. Ragauskas, T. Xia, H. Han, J. Tang, H. Yu, B. Xu, L. Peng, Single-molecular insights into the breakpoint of cellulose nanofibers assembly during saccharification, *Nat. Commun.* 14 (1) (2023) 1100, <https://doi.org/10.1038/s41467-023-36856-8>.
- S. Praveen, J. Jegan, T. Bhagavathi Pushpa, R. Gokulan, L. Bulgariu, Biochar for removal of dyes in contaminated water: an overview, *Biochar* 4 (1) (2022) 10, <https://doi.org/10.1007/s42773-022-00131-8>.
- A. Soudani, L. Youcef, L. Bulgariu, S. Youcef, K. Toumi, N. Soudani, Characterizing and modeling of oak fruit shells biochar as an adsorbent for the removal of Cu, Cd, and Zn in single and in competitive systems, *Chem. Eng. Res. Des.* 188 (2022) 972–987, <https://doi.org/10.1016/j.cherd.2022.10.009>.
- C. Zhang, G. Zeng, D. Huang, C. Lai, M. Chen, M. Cheng, W. Tang, L. Tang, H. Dong, B. Huang, X. Tan, R. Wang, Biochar for environmental management: mitigating greenhouse gas emissions, contaminant treatment, and potential negative impacts, *Chem. Eng. J.* 373 (2019) 902–922, <https://doi.org/10.1016/j.cej.2019.05.139>.
- M.R. Barr, L. Forster, C. D'Agostino, R. Volpe, Alkaline pretreatment of walnut shells increases pore surface hydrophilicity of derived biochars, *Appl. Surf. Sci.* 571 (2022) 151253, <https://doi.org/10.1016/j.apsusc.2021.151253>.
- T. Li, H. Peng, B. He, C. Hu, H. Zhang, Y. Li, Y. Yang, Y. Wang, M.M.A. Bakr, M. Zhou, L. Peng, H. Kang, Cellulose de-polymerization is selective for bioethanol refinery and multi-functional biochar assembly using brittle stalk of corn mutant, *Int. J. Biol. Macromol.* 264 (2024) 130448, <https://doi.org/10.1016/j.ijbiomac.2024.130448>.
- M. Wang, Y. Wang, J. Liu, H. Yu, P. Liu, Y. Yang, D. Sun, H. Kang, Y. Wang, J. Tang, C. Fu, L. Peng, Integration of advanced biotechnology for green carbon, *Green Carbon* (2024), <https://doi.org/10.1016/j.greenca.2024.02.006>.
- L. Cheng, L. Wang, L. Wei, Y. Wu, A. Alam, C. Xu, Y. Wang, Y. Tu, L. Peng, T. Xia, Combined mild chemical pretreatments for complete cadmium release and cellulosic ethanol co-production distinctive in wheat mutant straw, *Green Chem.* 21 (13) (2019) 3693–3700, <https://doi.org/10.1039/C9GC00686A>.
- M. Hu, H. Yu, Y. Li, A. Li, Q. Cai, P. Liu, Y. Tu, Y. Wang, R. Hu, B. Hao, L. Peng, T. Xia, Distinct polymer extraction and cellulose DP reduction for complete cellulose hydrolysis under mild chemical pretreatments in sugarcane, *Carbohydr. Polym.* 202 (2018) 434–443, <https://doi.org/10.1016/j.carbpol.2018.08.039>.
- V. Kumar, S.K. Yadav, J. Kumar, V. Ahluwalia, A critical review on current strategies and trends employed for removal of inhibitors and toxic materials generated during biomass pretreatment, *Bioresour. Technol.* 299 (2020) 122633, <https://doi.org/10.1016/j.biortech.2019.122633>.
- Z. Lv, F. Liu, Y. Zhang, Y. Tu, P. Chen, L. Peng, Ecologically adaptable *Populus simonii* is specific for recalcitrance-reduced lignocellulose and largely enhanced enzymatic saccharification among woody plants, *GCB Bioenergy* 13 (2) (2021) 348–360, <https://doi.org/10.1111/gcbb.12764>.
- F. Li, G. Xie, J. Huang, R. Zhang, Y. Li, M. Zhang, Y. Wang, A. Li, X. Li, T. Xia, C. Qu, F. Hu, A.J. Ragauskas, L. Peng, OsCESA9 conserved-site mutation leads to largely enhanced plant lodging resistance and biomass enzymatic saccharification by reducing cellulose DP and crystallinity in rice, *Plant Biotechnol. J.* 15 (9) (2017) 1093–1104, <https://doi.org/10.1111/pbi.12700>.
- R. Zhang, H. Hu, Y. Wang, Z. Hu, S. Ren, J. Li, B. He, Y. Wang, T. Xia, P. Chen, G. Xie, L. Peng, A novel rice *fragile culm 24* mutant encodes a UDP-glucose epimerase that affects cell wall properties and photosynthesis, *J. Exp. Bot.* 71 (10) (2020) 2956–2969, <https://doi.org/10.1093/jxb/eraa044>.
- J. Huang, Y. Li, Y. Wang, Y. Chen, M. Liu, Y. Wang, R. Zhang, S. Zhou, J. Li, Y. Tu, B. Hao, L. Peng, T. Xia, A precise and consistent assay for major wall polymer features that distinctively determine biomass saccharification in transgenic rice by near-infrared spectroscopy, *Biotechnol. Biofuels* 10 (1) (2017) 294, <https://doi.org/10.1186/s13068-017-0983-x>.
- A. Sluiter, H. Hames, R. Ruiz, C. Scarlata, J. Sluiter, D. Templeton, D. Crocker, Determination of structural carbohydrates and lignin in biomass, *Laboratory Analytical Procedure* 1617 (1) (2008) 1–16.
- N. Xu, W. Zhang, S. Ren, F. Liu, C. Zhao, H. Liao, Z. Xu, J. Huang, Q. Li, Y. Tu, B. Yu, Y. Wang, J. Jiang, J. Qin, L. Peng, Hemicelluloses negatively affect lignocellulose crystallinity for high biomass digestibility under NaOH and H₂SO₄ pretreatments in *Miscanthus*, *Biotechnol. Biofuels* 5 (1) (2012) 58, <https://doi.org/10.1186/1754-6834-5-58>.
- Z. Hu, H. Peng, J. Liu, H. Zhang, S. Li, H. Wang, Z. Lv, Y. Wang, D. Sun, J. Tang, L. Peng, Y. Wang, Integrating genetic-engineered cellulose nanofibrils of rice straw with mild chemical treatments for enhanced bioethanol conversion and bioaerogels production, *Ind. Crop. Prod.* 202 (2023) 117044, <https://doi.org/10.1016/j.indcrop.2023.117044>.
- W. Zhang, Z. Yi, J. Huang, F. Li, B. Hao, M. Li, S. Hong, Y. Lv, W. Sun, A. Ragauskas, F. Hu, J. Peng, L. Peng, Three lignocellulose features that distinctively affect biomass enzymatic digestibility under NaOH and H₂SO₄ pretreatments in *Miscanthus*, *Bioresour. Technol.* 130 (2013) 30–37, <https://doi.org/10.1016/j.biortech.2012.12.029>.
- Z. Zheng, Q. Huang, C. Ling, Water-soluble yeast β -glucan fractions with different chromatic weights: extraction and separation by acidolysis assisted-size exclusion chromatography and their association with proliferative activity, *Int. J. Biol. Macromol.* 123 (2019) 269–279, <https://doi.org/10.1016/j.ijbiomac.2018.11.020>.
- Y. Li, J. Zhuo, P. Liu, P. Chen, H. Hu, Y. Wang, S. Zhou, Y. Tu, L. Peng, Y. Wang, Distinct wall polymer deconstruction for high biomass digestibility under chemical pretreatment in *Miscanthus* and rice, *Carbohydr. Polym.* 192 (2018) 273–281, <https://doi.org/10.1016/j.carbpol.2018.03.013>.
- B. Yang, C. Voiniciuc, L. Fu, S. Dieluweit, H. Klose, B. Usadel, TRM4 is essential for cellulose deposition in *Arabidopsis* seed mucilage by maintaining cortical microtubule organization and interacting with CESAs3, *New Phytol.* 221 (2) (2019) 881–895, <https://doi.org/10.1111/nph.15442>.
- Z. Hu, Q. Li, Y. Chen, T. Li, Y. Wang, R. Zhang, H. Peng, H. Wang, Y. Wang, J. Tang, M. Nauman Aftab, L. Peng, Intermittent ultrasound retains cellulases unlock for enhanced cellulosic ethanol with high-porosity biochar for dye adsorption using desirable rice mutant straw, *Bioresour. Technol.* 369 (2023) 128437, <https://doi.org/10.1016/j.biortech.2022.128437>.
- T.M. Pérez-Millán, D.I. Mendoza-Castillo, I.A. Aguayo-Villarreal, C.K. Rojas-Mayorga, F. Villanueva-Mejía, A. Bonilla-Petriciolet, Application of DFT and response surface models to analyze the adsorption process of basic blue 3 and reactive blue 19 dyes on sugarcane bagasse and coconut endocarp biomass, *J. Mol. Struct.* 1287 (2023) 135658, <https://doi.org/10.1016/j.molstruc.2023.135658>.
- H. Yu, M. Hu, Z. Hu, F. Liu, H. Yu, Q. Yang, H. Gao, C. Xu, M. Wang, G. Zhang, Y. Wang, T. Xia, L. Peng, Y. Wang, Insights into pectin dominated enhancements for elimination of toxic Cd and dye coupled with ethanol production in desirable lignocelluloses, *Carbohydr. Polym.* 286 (2022) 119298, <https://doi.org/10.1016/j.carbpol.2022.119298>.
- M. Jain, S.A. Khan, A. Sahoo, P. Dubey, K.K. Pant, Z.M. Ziora, M.A.T. Blaskovich, Statistical evaluation of cow-dung derived activated biochar for phenol adsorption: adsorption isotherms, kinetics, and thermodynamic studies, *Bioresour. Technol.* 352 (2022) 127030, <https://doi.org/10.1016/j.biortech.2022.127030>.
- V. Bharti, K. Vikrant, M. Goswami, H. Tiwari, R.K. Sonwani, J. Lee, D.C.W. Tsang, K.-H. Kim, M. Saeed, S. Kumar, B.N. Rai, B.S. Giri, R.S. Singh, Biodegradation of methylene blue dye in a batch and continuous mode using biochar as packing media, *Environ. Res.* 171 (2019) 356–364, <https://doi.org/10.1016/j.envres.2019.01.051>.
- C. Fan, S. Feng, J. Huang, Y. Wang, L. Wu, X. Li, L. Wang, Y. Tu, T. Xia, J. Li, X. Cai, L. Peng, AtCESA8-driven OsSUS3 expression leads to largely enhanced biomass saccharification and lodging resistance by distinctively altering lignocellulose features in rice, *Biotechnol. Biofuels* 10 (1) (2017) 221, <https://doi.org/10.1186/s13068-017-0911-0>.
- Q. Yang, X. Mei, Z. Wang, X. Chen, R. Zhang, Q. Chen, J. Kan, Comprehensive identification of non-volatile bitter-tasting compounds in *Zanthoxylum bungeanum* maxim. By untargeted metabolomics combined with sensory-guided fractionation technique, *Food Chem.* 347 (2021) 129085, <https://doi.org/10.1016/j.foodchem.2021.129085>.
- Y. Yuan, J. Xiao, M. Yilmaz, T.C. Zhang, S. Yuan, N. P. co-doped porous biochar derived from cornstalk for high performance CO₂ adsorption and electrochemical energy storage, *Sep. Purif. Technol.* 299 (2022) 121719, <https://doi.org/10.1016/j.seppur.2022.121719>.

- [38] P. Sarkar, E. Bosneaga, M. Auer, Plant cell walls throughout evolution: towards a molecular understanding of their design principles, *J. Exp. Bot.* 60 (13) (2009) 3615–3635, <https://doi.org/10.1093/jxb/erp245>.
- [39] F. Li, S. Ren, W. Zhang, Z. Xu, G. Xie, Y. Chen, Y. Tu, Q. Li, S. Zhou, Y. Li, F. Tu, L. Liu, Y. Wang, J. Jiang, J. Qin, S. Li, Q. Li, H.-C. Jing, F. Zhou, N. Gutterson, L. Peng, Arabinose substitution degree in xylan positively affects lignocellulose enzymatic digestibility after various NaOH/ H₂SO₄ pretreatments in *Miscanthus*, *Bioresour. Technol.* 130 (2013) 629–637, <https://doi.org/10.1016/j.biortech.2012.12.107>.
- [40] M. Pauly, S. Gille, L. Liu, N. Mansoori, A. de Souza, A. Schultink, G. Xiong, Hemicellulose biosynthesis, *Planta* 238 (4) (2013) 627–642, <https://doi.org/10.1007/s00425-013-1921-1>.
- [41] X. He, Z. Liu, W. Niu, L. Yang, T. Zhou, D. Qin, Z. Niu, Q. Yuan, Effects of pyrolysis temperature on the physicochemical properties of gas and biochar obtained from pyrolysis of crop residues, *Energy* 143 (2018) 746–756, <https://doi.org/10.1016/j.energy.2017.11.062>.
- [42] J. Li, Y. Li, Y. Wu, M. Zheng, A comparison of biochars from lignin, cellulose and wood as the sorbent to an aromatic pollutant, *J. Hazard. Mater.* 280 (2014) 450–457, <https://doi.org/10.1016/j.jhazmat.2014.08.033>.
- [43] Z. Li, C. Zhao, Y. Zha, C. Wan, S. Si, F. Liu, R. Zhang, F. Li, B. Yu, Z. Yi, N. Xu, L. Peng, Q. Li, The Minor Wall-networks between Monolignols and interlinked-Phenolics predominantly affect biomass enzymatic digestibility in *Miscanthus*, *PLoS One* 9 (8) (2014) e105115, <https://doi.org/10.1371/journal.pone.0105115>.
- [44] P.A. Penttilä, A. Várnai, J. Pere, T. Tammelin, L. Salmén, M. Siika-aho, L. Viikari, R. Serimaa, Xylan as limiting factor in enzymatic hydrolysis of nanocellulose, *Bioresour. Technol.* 129 (2013) 135–141, <https://doi.org/10.1016/j.biortech.2012.11.017>.
- [45] M.J. Ahmed, P.U. Okoye, E.H. Hummadi, B.H. Hameed, High-performance porous biochar from the pyrolysis of natural and renewable seaweed (*Gelidium acerosa*) and its application for the adsorption of methylene blue, *Bioresour. Technol.* 278 (2019) 159–164, <https://doi.org/10.1016/j.biortech.2019.01.054>.
- [46] X. Zhang, B. Gao, Y. Zheng, X. Hu, A.E. Creamer, M.D. Annable, Y. Li, Biochar for volatile organic compound (VOC) removal: sorption performance and governing mechanisms, *Bioresour. Technol.* 245 (2017) 606–614, <https://doi.org/10.1016/j.biortech.2017.09.025>.
- [47] Z. Zhang, Z.P. Cano, D. Luo, H. Dou, A. Yu, Z. Chen, Rational design of tailored porous carbon-based materials for CO₂ capture, *J. Mater. Chem. A* 7 (37) (2019) 20985–21003, <https://doi.org/10.1039/C9TA07297G>.
- [48] L. Qi, X. Tang, Z. Wang, X. Peng, Pore characterization of different types of coal from coal and gas outburst disaster sites using low temperature nitrogen adsorption approach, *Int. J. Min. Sci. Technol.* 27 (2) (2017) 371–377, <https://doi.org/10.1016/j.ijmst.2017.01.005>.
- [49] R. Bardestani, S. Kaliaguine, Steam activation and mild air oxidation of vacuum pyrolysis biochar, *Biomass Bioenergy* 108 (2018) 101–112, <https://doi.org/10.1016/j.biombioe.2017.10.011>.
- [50] Q. Hu, Y. Zhu, B. Hu, S. Lu, G. Sheng, Mechanistic insights into sequestration of U (VI) toward magnetic biochar: batch, XPS and EXAFS techniques, *J. Environ. Sci.* 70 (2018) 217–225, <https://doi.org/10.1016/j.jes.2018.01.013>.
- [51] Y. Ai, H. Wang, P. Liu, H. Yu, M. Sun, R. Zhang, J. Tang, Y. Wang, S. Feng, L. Peng, Insights into contrastive cellulose nanofibrils assembly and nanocrystals catalysis from dual regulations of plant cell walls, *Sci. Bull.* (2024), <https://doi.org/10.1016/j.scib.2024.06.013>.